

Received June 1, 2020, accepted July 1, 2020, date of publication July 6, 2020, date of current version July 17, 2020.

Digital Object Identifier 10.1109/ACCESS.2020.3007204

Image Inpainting by Low-Rank Prior and Iterative Denoising

RUYI HAN¹, SHUMEI WANG², SHUJUN FU¹, YULIANG LI³, SHOUYI LIU⁴, AND WEIFENG ZHOU⁵

¹School of Mathematics, Shandong University, Jinan 250100, China

²The First Department of General Surgery, Yidu Central Hospital of Weifang, Qingzhou 262500, China

³Department of Intervention Medicine, The Second Hospital of Shandong University, Jinan 250033, China

⁴Department of Electrical and Electronic Engineering, Xi'an Jiaotong-Liverpool University, Suzhou 215123, China

⁵School of Mathematics and Physics, Qingdao University of Science and Technology, Qingdao 266071, China

Corresponding author: Shujun Fu (shujunfu@163.com)

This work was supported in part by the National Natural Science Foundation of China under Grant 61671276 and Grant 11971269, in part by the Natural Science Foundation of Shandong Province of China under Grant ZR2019MF045, in part by the Qingdao source innovation project under Grant 18-2-2-64-jch, and in part by the Science and Technology Program of Universities of Shandong Province under Grant J18KA314.

ABSTRACT To reconstruct the missing or damaged parts of images from observed incomplete data, some traditional methods have been researched in recent years. The iterative denoising and backward projections(IDBP)algorithm with a simple parameter mechanism have been recently introduced, which solves the typical inverse problem by utilizing the existing 3D transform-domain collaborative filtering denoising algorithm(BM3D). While this algorithm has simple parameter tuning, the collaborative hard-thresholding applied to the 3D group is greatly restricted in the procedure of denoising. In this paper, we remedy this deficiency using an iteration reweighted shrinkage denoising method. First, the model is obtained by a Plug and Play(P&P) framework. Then, we solve the optimization problem by using a proposed denoising model based on low rank prior and reweighted shrinkage and obtain a closed-form solution. Finally, the closed-form solution is operated iteratively by using the adaptive backward projection technique. Utilizing this novel strategy, the proposed algorithm not only removes the image noise and effectively recovers the degraded image, but also preserves fine structure and texture information of the image. Experimental results indicate that the proposed algorithm is competitive with some state-of-the-art inpainting algorithms in terms of both numerical evaluation and visual quality.

INDEX TERMS Image inpainting, iterative denoising, inverse problem, singular value shrinkage, low-rank prior.

I. INTRODUCTION

Image inpainting has developed rapidly in recent years. It is one of the research hotspots in the field of image processing. Image inpainting plays an important role in machine learning [1], computer vision [2], control [3] and other information fields. And image inpainting is also used in system recognition [4] and multi-task learning [5].

Image inpainting is a typical ill-posed inverse problem, which aims to reconstruct the missing or damaged parts of the images from observed incomplete data matrix as accurate as possible. Finally, the degraded image is filled. This discomfort causes its solution not to be unique. Therefore, it is very

The associate editor coordinating the review of this manuscript and approving it for publication was Peng Liu¹.

necessary to introduce some reasonable prior information when solving the inpainting optimization problem.

Solving the problem of image inpainting [6]–[11] based on the low-rank property of image has attracted increasing interest in recent years. The low rank prior to the image assumes that the image can be represented by a low-rank matrix. Based on this assumption, the image inpainting problem can be described as a low-rank matrix approximation problem. It is described as the following rank minimization model:

$$\begin{aligned} & \min \text{rank}(X) \\ & \text{s.t. } X_{ij} = M_{ij}, (i, j) \in \Omega \end{aligned} \quad (1)$$

where $X \in \mathbb{R}^{n_1 \times n_2}$, $M \in \mathbb{R}^{n_1 \times n_2}$ and M is observed incomplete data matrix, $\Omega \subset \{1, \dots, n_1\} \times \{1, \dots, n_2\}$ is the subscript set of the known elements of the data matrix.

In the early years, experts proposed many algorithms to solve the problem (1), such as the Riemannian trust-region method(RTRMC) [12], OptSpace algorithm [13], ADMiRA algorithm [14]. Then, Lu found that all the existing nonconvex penalty functions are concave and monotonically increasing on $[0, \infty]$, and their gradients are decreasing functions. Based on this property, Lu proposed nonconvex nonsmooth low-rank minimization algorithm(IRNN) [15].

Since the rank function is nonconvex and discontinuous, problem (1) is NP-hard. Candès and Recht [16] carried out convex relaxation optimization on the problem (1), obtained the following nuclear norm minimization model:

$$\begin{aligned} & \min \|X\|_* \\ & \text{s.t. } X_{ij} = M_{ij}, \quad (i, j) \in \Omega \end{aligned} \quad (2)$$

where $\|X\|_*$ denotes the nuclear norm and is defined by the sum of singular values of X , the formula is expressed as $\|X\|_* = \sum_{k=1}^r \sigma_k(X)$, $\text{rank}(X) = r$, $\sigma_k(X)$ denotes the k -th singular value of the matrix X .

Then, many algorithms were proposed to solve the problem (2), such as the accelerated proximal gradient algorithm (APG) [17], and the singular value thresholding algorithm (SVT) [18], the augmented Lagrange multiplier algorithm(ALM) [19], more algorithms can reference [20]–[26].

After singular value decomposition of the matrix, each singular value has a specific physical meaning, so they should be treated unequally in the process of a singular value threshold. However, in many traditional methods, these singular values are treated equally. Another danger in these traditional methods is that it is computationally expensive because it needs to compute the singular value decomposition(SVD)of a matrix at each iteration and the rank of a matrix is difficult to estimate. Recently, Guo proposed an effective rank estimation method, which is a two-stage low-rank approximation(TSLRA) [27]. This algorithm avoided the expensive singular value decomposition in calculation combined with the truncated singular value method effectively.

In recent years, a new method of image inpainting has attracted the attention of many researchers. Inspired by Plug-and-Play framework [28], Tom and Raja proposed iterative denoising and backward projections(IDBP-BM3D) [29] algorithm, they used an image denoising method to solve the image inpainting problem. This method overcomes Plug-and-Play's shortages of expensive iteration costs and unclear parameters. The most important thing is that the experimental results are better than Plug and Play. In this paper, we improve the IDBP-BM3D method by using the low-rank prior to the image and assigning different weights to the singular values of the matrix in the iterative process by combining the reweighted shrinkage method [30]. Finally, we obtain high-quality inpainting results. Extensive experimental results demonstrate the feasibility and effectiveness of our method.

The rest part of this paper is organized as follows. Section II introduces some related works. Section III describes the proposed method. Section IV applies the proposed method to image inpainting and compares our method with other inpainting methods, and the experiment results prove that our method is feasible and effective. Section V concludes this paper.

II. RELATED WORK

A. IMAGE INPAINTING

The problem of image inpainting aim to reconstruct the original image x from its degraded image y , this can be generally formulated by

$$y = Hx + e \quad (3)$$

where $x \in R^n$ denotes the unknown original image, $y \in R^m$ represents the degraded image, $H \in R^{m \times n}$ is degradation matrix and $e \in R^m$ is a vector of independent and identically distributed Gaussian random variables with zero mean and the standard deviation of σ_e .

In all cases of image degradation, accurately estimating the original matrix x from the degraded matrix y is equivalent to solving an ill-posed inverse problem. Therefore, it is very necessary to introduce reasonable prior information $s(x)$ when solving the inpainting optimization problem. In the image inpainting problem, the degradation factor H is a full row rank matrix. Hence, after the discussion of this paper, we assume $m < n$.

In almost many image inpainting methods, the process of estimating the original image above is formulated as a problem of solving the energy function. The energy function is composed of fidelity term $\frac{1}{2\sigma_e^2} \|y - Hx\|_2^2$ is normalized by the noise variance $2\sigma_e^2$ and penalty term. The penalty term regularizes the optimization problem through the reasonable prior information $s(x)$. Thus, the typical energy function is expressed as

$$f(x) = \frac{1}{2\sigma_e^2} \|y - Hx\|_2^2 + s(x), \quad (4)$$

where x is the optimal solution of the energy function, and $\|\cdot\|_2$ stands for the Euclidean norm. For the completeness of this paper, we briefly introduce the two algorithms in Part B. PLUG AND PLAY METHOD and Part C. IDBP METHOD.

B. PLUG AND PLAY METHOD

As described in part A above, the image inpainting problem becomes a problem of minimizing the energy function, namely, $\min_x f(x)$. Then the Plug and Play method is proposed to solve this minimization problem.

By separating variables, rewrite the problem (4) as the following minimization problem

$$\min_{x,v} l(x) + \beta s(v) \quad \text{s.t. } x = v, \quad (5)$$

where $l(x) \triangleq \frac{1}{2\sigma_e^2} \|y - Hx\|_2^2$ is the fidelity term in (4), and β is a positive parameter.

Constructing the augmented Lagrange function of (5), which is given by

$$L_\lambda = l(x) + \beta s(v) + u^T(x - v) + \frac{\lambda}{2} \|x - v\|_2^2, \quad (6)$$

where u denotes lagrange multiplier, λ represents penalty parameter.

By using ADMM [31] algorithm to solve (6), we obtain the following solution

$$\begin{aligned} x_k &= \arg \min_x l(x) + \frac{\lambda}{2} \|x - (v_{k-1} - u_{k-1})\|_2^2, \\ v_k &= \arg \min_v \frac{\lambda}{2\beta} \|(x_k + u_{k-1}) - v\|_2^2 + s(v), \\ u_k &= u_{k-1} + (x_k - v_k). \end{aligned} \quad (7)$$

The Plug and Play algorithm is presented in Algorithm 1.

Algorithm 1 Plug and Play

Input: H , y , σ_e , denoising operator $D(\cdot, \sigma)$, stopping criterion; $y = Hx + e$, such that $e \sim N(0, \sigma_e^2 I_m)$, x is an unknown signal whose prior model is specified by $D(\cdot, \sigma)$.

Output: \hat{x} an estimate for x .

- 1: Initialize $v_0, \beta, \lambda, u_0 = 0, k = 0$;
 - 2: **while** stopping criterion not met **do**
 - 3: $k = k + 1$;
 - 4: $x_k = (H^T H + \lambda \sigma_e^2 I_n)^{-1} \times (H^T y + \lambda \sigma_e^2 (v_{k-1} - u_{k-1}))$;
 - 5: $v_k = D(x_k + u_{k-1}; \sqrt{\beta/\lambda})$;
 - 6: $u_k = u_{k-1} + (x_k - v_k)$;
 - 7: **end while**
 - 8: $\hat{x} = x_k$.
-

Although Plug and Play method can complete the task of image inpainting, in the experiment we found that this method costs a large number of iterations. The parameters β and λ not always clear. These elements will directly affect the quality of the filled images finally.

C. IDBP METHOD

Inspired by the Plug and Play method, Tom and Raja proposed IDBP algorithm, they used image denoising method BM3D to solve the image inpainting problem. They deformed the energy function (4) as follows:

$$f(x) = \frac{1}{2\sigma_e^2} \|H^\dagger y - x\|_{H^T H}^2 + s(x), \quad (8)$$

where

$$H^\dagger \triangleq H^T (H H^T)^{-1} \quad (9)$$

$$\|u\|_{H^T H}^2 \triangleq u^T H^T H u \quad (10)$$

where H^\dagger denotes the pseudo-inverse of the full row rank matrix H , and $\|u\|_{H^T H}$ is a semi-norm rather than a real norm.

Then, the problem of minimizing the energy function, namely, $\min_x f(x)$ can be rewritten as

$$\min_{x,y} \frac{1}{2\sigma_e^2} \|y - x\|_{H^T H}^2 + s(x), \quad s.t. y = H^\dagger y_0 \quad (11)$$

where y_0 refers to the degraded image.

Tom and Raja modified (11) to the following minimization problem

$$\min_{x,y} \frac{1}{2(\sigma_e + \delta)^2} \|y - x\|_2^2 + s(x), \quad s.t. H y = y_0 \quad (12)$$

where δ represents a tradeoff parameter.

By using alternating minimization method, the solution x_k of (12) is estimated by solving

$$x_k = \arg \min_x \frac{1}{2(\sigma_e + \delta)^2} \|y_{k-1} - x\|_2^2 + s(x), \quad (13)$$

$$y_k = \arg \min_y \|y - x_k\|_2^2 \quad s.t. H y = y_0, \quad (14)$$

The closed-form solution of (14) is obtained by using the affine subspace projection technique,

$$y_k = H^\dagger y + (I_n - H^\dagger H)x_k. \quad (15)$$

The IDBP algorithm is presented in Algorithm 2.

Algorithm 2 IDBP

Input: H , y_0 , σ_e , denoising operator $D(\cdot, \sigma)$, stopping criterion; $y_0 = Hx + e$, such that $e \sim N(0, \sigma_e^2 I_m)$, x is an unknown signal whose prior model is specified by $D(\cdot, \sigma)$.

Output: \hat{x} an estimate for x .

- 1: Initialize $y_0, \delta, k = 0$;
 - 2: **while** stopping criterion not met **do**
 - 3: $k = k + 1$;
 - 4: $x_k = D(y_{k-1}; \sigma_e + \delta)$;
 - 5: $y_k = H^\dagger y_0 + (I_n - H^\dagger H)x_k$;
 - 6: **end while**
 - 7: $\hat{x} = x_k$.
-

In the comparison experiment between the following algorithms, the IDBP algorithm here uses the BM3D denoising method. We called IDBP-BM3D.

In the IDBP-BM3D algorithm, the prior information $s(x)$ is selected adaptively in the BM3D denoising method. And the collaborative hard-thresholding applied to the 3D group is greatly restricted in the procedure of denoising. In fact, in the process of singular value shrinkage of the low-rank matrix, each singular value has definite practical meanings, so they should be treated differently. Therefore, in the following discussion, we propose an iterative reweighted shrinkage denoising method to improve this deficiency, and we apply this skill to the IDBP inpainting method.

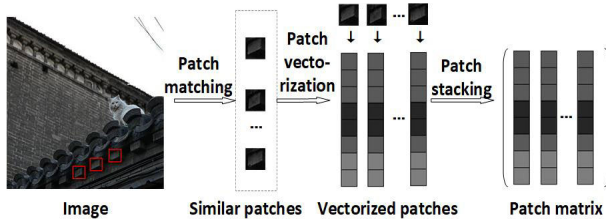


FIGURE 1. Flowchart of the constructed low-rank patch matrix.

III. PROPOSED METHOD

A. LOW RANK PRIOR

In recent years, the application of low-rank priors in image processing tasks has attracted great attention from many scholars, such as denoising, deblurring, and image completion. The data matrix of a clear natural image is usually low rank or approximately low rank. A low rank means that the rank of the matrix is relatively small, while the low-rank property of the matrix means that the rank of the matrix is relatively small compared to the number of rows or columns of the matrix.

An image can be viewed as a matrix. According to the definition of the rank of the matrix, the fewer bases in a matrix, the fewer linearly independent vectors, and the smaller the rank of the matrix. When the rank is much smaller than the size of the matrix, the image is called low-rank. Each row or column of a matrix can be represented linearly with other rows or columns. This indicates that the matrix contains a large amount of redundant information, which can be used to recover the information in the real image. In image processing, rank can be interpreted as the richness of information contained in the image. Therefore, the low-rank prior information of the image can be used to remove the noise in the image and fill in the missing pixels.

In the proposed method, we use the block matching method to construct the low-rank block matrix of the image. When looking for similar blocks of the target block, Euclidean distance will serve as the measuring mechanism. Fig.1 shows a specific flowchart for constructing the low-rank patch matrix of the image.

B. ITERATION REWEIGHTED SHRINKAGE DENOISING

Definition 1 (Singular Value Decomposition): Given $X \in R^{n^1 \times n^2}$, and the rank is r . There must be orthogonal matrices $U \in R^{n^1 \times r}$ and $V \in R^{n^2 \times r}$, such that

$$X = U \Sigma_r V^T, \quad \Sigma_r = \text{diag}(\sigma_1, \sigma_2, \dots, \sigma_r) \quad (16)$$

where σ_i represents the singular value of matrix X , and $\sigma_1 \geq \sigma_2 \geq \dots \geq \sigma_r > 0$

Definition 2 [18] (The Singular Value Shrinkage Operator): For any parameter $\tau \geq 0$, the matrix $X \in R^{n^1 \times n^2}$, and the rank is r . Singular value decomposition of the matrix X exists, $X = U \Sigma_r V^T$, singular threshold operator D_τ is defined as follows:

$$D_\tau(X) = U D_\tau(\Sigma) V^T, \quad D_\tau(\Sigma) = \text{diag}((\sigma_i - \tau)_+), \quad (17)$$

where σ_i represents the singular value of matrix X . And

$$(\sigma_i - \tau)_+ = \begin{cases} \sigma_i - \tau, & \text{if } \sigma_i > \tau \\ 0, & \text{if } \sigma_i \leq \tau. \end{cases}$$

In IDBP-BM3D algorithm, the denoising algorithm BM3D processes prior information adaptively through the cassette. And applied the collaborative hard-thresholding to the 3D group in the procedure of denoising. In the image processing task, although the large singular value corresponds to more important information in the image, for the complex image, the small singular value may contain more subtle and rich texture details of the image. If those small singular values are simply understood as noise and removed, the integrity of the image may be affected, especially the restoration effect of image edges and textures may not be very good. Therefore, this greatly restricts its capability and flexibility in image denoising. Singular values often correspond to the important information hidden in the matrix, and the importance is positively correlated with the size of singular values. Every matrix A can be represented as the sum of a series of small matrices of rank one, this singular values measure the importance of these small matrices to A .

Based on the previous part of low-rank prior information, Eq. (13) is equivalent to the following minimization problem

$$\hat{X} = \arg \min_X \frac{1}{2(\sigma_e + \delta)^2} \|Y - X\|_F^2 + \|X\|_* \quad (18)$$

Note that δ is a tradeoff parameter. In order to obtain high quality inpainting result, we apply the reweighting mechanism and assign different weight ω_i to each singular value $\sigma_i(X)$, the i -th singular value of X , We let the reweighting the formula as follows:

$$\omega_i = c\sqrt{n}/(\sigma_i(X) + \epsilon), \quad (19)$$

where $c > 0$ is a constant, n is the number of similar patches in Y , ϵ is a small constant. And the initial $\sigma_i(X)$ can be estimated as

$$\hat{\sigma}_i(X) = \sqrt{\max(\sigma_i^2(Y) - 2n(\sigma_e + \delta)^2)},$$

where $\sigma_i(Y)$ is the i -th singular value of Y .

Therefore, the solution of minimization problem (13) is finally obtained by solving the following equation:

$$\hat{X} = \arg \min_X \frac{1}{2(\sigma_e + \delta)^2} \|Y - X\|_F^2 + \|X\|_{\omega,*} \quad (20)$$

Lemma 1 [32](Von Neumanns Trace Inequality): For any $m \times n$ matrices A and B , $\text{tr}(A^T B) \leq \sum_i \sigma_i(A) \sigma_i(B)$, where $\Sigma_1(A) \geq \Sigma_2(A) \geq \dots \geq 0$ and $\Sigma_1(B) \geq \Sigma_2(B) \geq \dots \geq 0$ are the descending singular values of A and B , respectively. The case of equality occurs if and only if it is possible to find unitaries U and V that simultaneously singular value decompose A and B in the sense that

$$A = U \Sigma_A V^T, \quad \text{and} \quad B = U \Sigma_B V^T,$$

where Σ_A and Σ_B denote the ordered eigenvalue matrices with singular value $\sigma(A)$ and $\sigma(B)$ along the diagonal with the same order, respectively.

The nonconvex problem (20) is transformed into a simple quadratic optimization problem to be solved by the following theorem 1.

Theorem 1: Given $Y \in R^{m \times n}$, we assume that $m \geq n$ and let $Y = U\Sigma V^T$ be the SVD of Y , where $\Sigma = \begin{pmatrix} \text{diag}(\sigma_1, \sigma_2, \dots, \sigma_n) \\ 0 \end{pmatrix} \in R^{m \times n}$. The global optimum of the problem (20) can be expressed as $X = UDV^T$, where $D = \begin{pmatrix} \text{diag}(d_1, d_2, \dots, d_n) \\ 0 \end{pmatrix}$ is a non-negative diagonal matrix and (d_1, d_2, \dots, d_n) is the solution to the following quadratic optimum problem:

$$\begin{aligned} \min_{d_i} \quad & \frac{1}{2(\sigma_e + \delta)^2} \sum_{i=1}^n ((d_i - \sigma_i)^2 + \omega_i d_i) \\ \text{s.t. } & d_1 \geq d_2 \geq \dots \geq d_n \geq 0 \end{aligned} \quad (21)$$

Proof: Let $X, Y \in R^{m \times n}$, $X = \bar{U}\bar{D}\bar{V}^T$ and $Y = U\Sigma V^T$ are the SVD of X and Y , respectively, where $\Sigma = \begin{pmatrix} \text{diag}(\sigma_1, \sigma_2, \dots, \sigma_n) \\ 0 \end{pmatrix} \in R^{m \times n}$ and $D = \begin{pmatrix} \text{diag}(d_1, d_2, \dots, d_n) \\ 0 \end{pmatrix}$ are diagonal singular value matrices. We have

$$\begin{aligned} & \frac{1}{2(\sigma_e + \delta)^2} \|Y - X\|_F^2 + \|X\|_{\omega,*} \\ &= \frac{1}{2(\sigma_e + \delta)^2} \langle Y - X, Y - X \rangle + \sum_{i=1}^n \omega_i d_i \\ &= \frac{1}{2(\sigma_e + \delta)^2} \text{tr}((Y - X)^T(Y - X)) + \sum_{i=1}^n \omega_i d_i \\ &= \frac{1}{2(\sigma_e + \delta)^2} (\text{tr}(Y^T Y) - 2\text{tr}(Y^T X) + \text{tr}(X^T X)) + \sum_{i=1}^n \omega_i d_i \\ &= \frac{1}{2(\sigma_e + \delta)^2} \left(\sum_{i=1}^n \sigma_i^2 - 2\text{tr}(Y^T X) + \sum_{i=1}^n d_i^2 \right) + \sum_{i=1}^n \omega_i d_i \\ &\geq \frac{1}{2(\sigma_e + \delta)^2} \left(\sum_{i=1}^n \sigma_i^2 - 2 \sum_{i=1}^n \sigma_i d_i + \sum_{i=1}^n d_i^2 \right) + \sum_{i=1}^n \omega_i d_i \\ &= \frac{1}{2(\sigma_e + \delta)^2} \sum_{i=1}^n (d_i - \sigma_i)^2 + \sum_{i=1}^n \omega_i d_i \end{aligned}$$

Therefore, this non-convex problem (20) can be solved by the quadratic optimization (21), and the solution is $X = UDV^T$, where D is the solution of the quadratic optimization problem (21).

End of proof.

Corollary 1: If $\sigma_1 \geq \dots \geq \sigma_n \geq 0$, and the weights are non-descending, then the global optimum of (21) is $d_i = \max(\sigma_i - (\sigma_e + \delta)^2 \omega_i, 0)$.

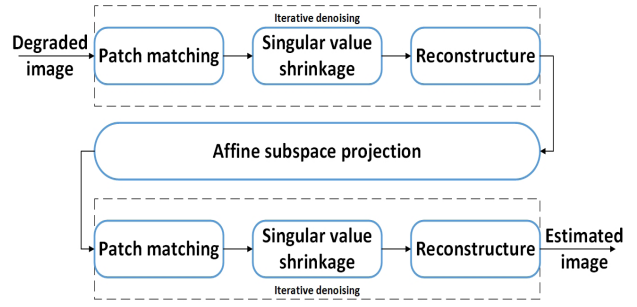


FIGURE 2. Flowchart of the proposed inpainting algorithm.

Proof: By definition 1 we know $\sigma_1 \geq \dots \geq \sigma_n$ and the weight vector has a non-descending order. we have

$$\begin{aligned} & \frac{1}{2(\sigma_e + \delta)^2} \sum_{i=1}^n (d_i - \sigma_i)^2 + \sum_{i=1}^n \omega_i d_i \\ &= \frac{1}{2(\sigma_e + \delta)^2} \left(\sum_{i=1}^n \sigma_i^2 - 2 \sum_{i=1}^n \sigma_i d_i \right. \\ &\quad \left. + \sum_{i=1}^n d_i^2 + 2(\sigma_e + \delta)^2 \omega_i d_i \right) \\ &= \frac{1}{2(\sigma_e + \delta)^2} \left(\sum_{i=1}^n d_i^2 - \sum_{i=1}^n (2\sigma_i - 2(\sigma_e + \delta)^2 \omega_i) d_i + \sum_{i=1}^n \sigma_i^2 \right) \\ &= \frac{1}{2(\sigma_e + \delta)^2} \sum_{i=1}^n \left(d_i - \frac{2\sigma_i - 2(\sigma_e + \delta)^2 \omega_i}{2} \right)^2 + k \\ &= \frac{1}{2(\sigma_e + \delta)^2} \sum_{i=1}^n (d_i - (\sigma_i - (\sigma_e + \delta)^2 \omega_i))^2 + k \end{aligned}$$

where k is a constant independent of d_i .

Then, this non-convex optimization problem can be replaced by a quadratic programming problem, and we can easily derive the global optimal solution is:

$$d_i = \max(\sigma_i - (\sigma_e + \delta)^2 \omega_i, 0)$$

End of proof.

The main procedures of this proposed method are exhibited in Fig.2.

This method effectively combines the low-rank prior information of the image and it approximates the image as a low-rank matrix, and assigns different weights to the singular value according to its importance in the image. Finally, these techniques improve the results of image restoration. The proposed method is shown in algorithm 3.

We obtain the solution \tilde{y}_k through the projection of \tilde{x}_k onto the affine subspace $HR^n = y$, update denoising component \tilde{y}_k , finally, the optimal estimate \tilde{x}_{k+1} is obtained.

Assuming that the result of the denoiser is x , we have

$$\begin{aligned} y_1 &= H^\dagger y + (I_n - H^\dagger H)x \\ &= H^\dagger(Hx + e) + (I_n - H^\dagger H)x \\ &= x + H^\dagger e \end{aligned} \quad (22)$$

Algorithm 3 Our Algorithm

Input: H, y, σ_e , stopping criterion; $y = Hx + e$, such that $e \sim N(0, \sigma_e^2)$ and x is an unknown signal.

Output: \hat{x} an estimate for x .

- 1: Initialize $\tilde{y}_0, \delta, \delta_0, n = 0, \tilde{x}_0 = \tilde{y}_0$;
- 2: **while** stopping criterion not met **do**
- 3: $n = n + 1$;
- 4: **for** $k = 1 : K$ **do**
- 5: Iterative regularization [33] $\tilde{y}_k = \tilde{x}_{k-1} + \delta_0(\tilde{y}_{n-1} - \tilde{x}_{k-1})$;
- 6: **for** each patch $\tilde{y}_{0,j}$ in \tilde{y}_k **do**
- 7: Find similar patch group Y_j ;
- 8: Estimate weight vector w ;
- 9: Singular value decomposition $[U, \Sigma, V] = SVD(Y_j)$;
- 10: Get the estimation: $\hat{X}_j = US_w(\Sigma)V^T$;
- 11: **end for**
- 12: Aggregate X_j to form the restored image \tilde{x}_k ;
- 13: **end for**
- 14: $\tilde{y}_n = H^\dagger y + (I_n - H^\dagger H)\tilde{x}_k$;
- 15: **end while**
- 16: $\hat{x} = \tilde{x}_k$.

Theorem 2: If $\lim_{k \rightarrow \infty} \|\tilde{x}_k - \tilde{x}_{k-1}\|_2 = 0$, then $\lim_{k \rightarrow \infty} \|\tilde{y}_k - y\|_2 - \lim_{k \rightarrow \infty} \|\tilde{y}_{k-1} - y\|_2 = 0$

Proof:

$$\begin{aligned}
 & \lim_{k \rightarrow \infty} \|\tilde{y}_k - y\|_2 \\
 &= \lim_{k \rightarrow \infty} \|H^\dagger y + (I_n - H^\dagger H)\tilde{x}_k - (x + H^\dagger e)\|_2 \\
 &= \lim_{k \rightarrow \infty} \|(I_n - H^\dagger H)\tilde{x}_k - (x - H^\dagger Hx)\|_2 \\
 &= \lim_{k \rightarrow \infty} \|(I_n - H^\dagger H)(\tilde{x}_k - x)\|_2 \\
 &= \lim_{k \rightarrow \infty} \|(I_n - H^\dagger H)(\tilde{x}_k - x)\|_2 \\
 &= \lim_{k \rightarrow \infty} \|(I_n - H^\dagger H)(\tilde{x}_{k-1} - x)\|_2 \\
 &= \lim_{k \rightarrow \infty} \|(I_n - H^\dagger H)\tilde{x}_{k-1} - x + H^\dagger Hx\|_2 \\
 &= \lim_{k \rightarrow \infty} \|(I_n - H^\dagger H)\tilde{x}_{k-1} - x + H^\dagger Hx - H^\dagger e + H^\dagger e\|_2 \\
 &= \lim_{k \rightarrow \infty} \|(I_n - H^\dagger H)\tilde{x}_{k-1} - (x + H^\dagger e) + H^\dagger(Hx + e)\|_2 \\
 &= \lim_{k \rightarrow \infty} \|(H^\dagger y + (I_n - H^\dagger H)\tilde{x}_{k-1} - (x + H^\dagger e))\|_2 \\
 &= \lim_{k \rightarrow \infty} \|\tilde{y}_{k-1} - y\|_2
 \end{aligned}$$

Therefore, we have $\lim_{k \rightarrow \infty} \|\tilde{y}_k - y\|_2 - \lim_{k \rightarrow \infty} \|\tilde{y}_{k-1} - y\|_2 = 0$.

End of proof.

IV. EXPERIMENTAL RESULTS

In this section, we test the proposed method on 12 widely used test images and compare our method with some advanced inpainting methods, including nonconvex nonsmooth low-rank

minimization algorithm(IRNN), two-stage low-rank approximation(TSLRA), Plug and Play method(P&P-BM3D) and iterative denoising and backward projections(IDBP-BM3D). For the completeness and credibility of the experiment, a recently developed deep learning-based image inpainting method, Deep Image Prior(DEEP) [34], is also used to compare with our method. In the process of denoising, the image is approximated to a low-rank matrix by block matching. In our experiment, we set the patch size to 12×12 . Gaussian white noise with a mean of zero and a standard deviation of 10 and 20 was added to these test images to generate the observational image. In the inpainting task, let the iterative regularization parameter $\delta_0 = 0.1$. To make the comparison clearer, all the missing cases are carried out with the same noise level in method.

A. IMAGE QUALITY METRICS

To fully evaluate the performance of the proposed algorithm, two metrics are used to quantify the reconstructed image quality. Including the peak signal-to-noise-ratio(PSNR) and structural similarity index measure(SSIM). The PSNR measures the quality of an image by calculating the size of the pixel error between the reconstructed image and the reference image. The larger the PSNR value, the smaller the distortion between the reconstructed image and the reference image, and the better the image quality. The SSIM describes the structural similarities between the reconstructed image and the reference image. The larger the SSIM value, the higher the similarity between the reconstructed image and the reference image. The calculation method of using PSNR and SSIM to characterize the image quality is as follows:

$$\begin{aligned}
 PSNR &= 10 \times \log_{10} \left(\frac{\max^2}{\frac{1}{N} \sum_{j=1}^n (I_j - \hat{I}_j)^2} \right) \\
 SSIM &= \frac{(2\mu_I\mu_{\hat{I}} + c_1)(2\sigma_I\sigma_{\hat{I}} + c_2)}{(\mu_I^2 + \mu_{\hat{I}}^2 + c_1)(\sigma_I^2 + \sigma_{\hat{I}}^2 + c_2)}
 \end{aligned}$$

where I is ground truth image, \hat{I} is reconstructed image; N and \max represent the number of pixels of the image and the maximum possible pixel value of the image respectively. μ_I and $\mu_{\hat{I}}$ are the average of I and \hat{I} , respectively; σ_I^2 and $\sigma_{\hat{I}}^2$ are the variance of I and \hat{I} , respectively; and $\sigma_I\sigma_{\hat{I}}$ is the covariance of I and \hat{I} . c_1 and c_2 are two constants, whose default values are 0.01 and 0.03.

B. EXPERIMENTAL RESULTS ON 12 TEST IMAGES

We evaluate the competing methods on 12 widely used test images, they are shown in Fig.3. The first 4 images are of size 256×256 , the last 3 images are of size 481×321 , and the other 5 images are of size 512×512 . All the experimental results are obtained in the MATLAB (R2018b) environment running on a PC with Intel(R) Core(TM) i7-8550U CPU @ 1.80GHz, and RAM 12.00 GB.

The PSNR results of these comparison algorithms are shown in Table 1 and the corresponding SSIM values are

**FIGURE 3.** The 12 test images used in image inpainting experiments.**TABLE 1.** PSNR results with 0.8 loss rate and noise level of 10.

	IRNN	TSLRA	P&P-BM3D	IDBP-BM3D	DEEP	Ours
<i>C.man</i>	22.48	24.82	23.80	24.68	21.91	24.93
<i>House</i>	27.25	29.87	28.79	31.62	28.60	32.14
<i>Peppers</i>	24.46	26.56	25.22	27.24	21.94	27.64
<i>Monarch</i>	22.16	25.25	24.46	25.53	21.22	26.02
<i>Lena</i>	27.54	29.89	28.11	30.14	27.58	30.82
<i>Barbara</i>	22.62	28.58	24.81	25.03	21.21	29.92
<i>Boat</i>	25.40	27.52	26.09	27.02	24.05	27.52
<i>Hill</i>	26.82	28.54	26.91	28.00	24.13	28.44
<i>Couple</i>	25.69	27.52	26.26	27.22	23.35	27.47
<i>Tiger</i>	23.36	25.23	24.17	24.60	22.95	25.02
<i>Zebra</i>	19.02	22.89	21.27	22.01	20.87	22.12
<i>Leopard</i>	24.26	25.30	24.31	25.26	23.67	25.36

shown in Table 2. The experimental data in Table 1 and Table 2 are the results at the noise level of 10, and the experimental data of the two indexes with a noise level of 20 are shown in Table 3 and Table 4. These four tables are the inpainting results of the image with a 0.8-pixel missing rate. All optimal results in the table are shown in bold font.

According to the numerical PSNR results in Table 1 and Table 3, the effect of IRNN, P&P-BM3D, and the DEEP algorithm is not as good as the other three methods. The PSNR results of our proposed algorithm are all better than the existing IDBP-BM3D algorithm. Even if the image is missing 80 percent of its pixels, it achieves 0.1-4.89dB improvement over the IDBP-BM3D algorithm on average. Although the PSNR results of the TSLRA algorithm are occasionally slightly higher than that of our method, with the increase of noise, the advantages of our algorithm become more prominent as shown in table 1 and table 3. From the SSIM metrics in table 2 and table 4, our algorithm is superior to all the comparison methods here.

TABLE 2. SSIM results with 0.8 loss rate and noise level of 10.

	IRNN	TSLRA	P&P-BM3D	IDBP-BM3D	DEEP	Ours
<i>C.man</i>	0.6235	0.7118	0.6452	0.7858	0.7176	0.8013
<i>House</i>	0.6739	0.7699	0.6894	0.8497	0.7920	0.8557
<i>Peppers</i>	0.7111	0.7846	0.7097	0.8291	0.4872	0.8388
<i>Monarch</i>	0.7227	0.8087	0.7458	0.8582	0.5854	0.8728
<i>Lena</i>	0.6827	0.7682	0.6860	0.8341	0.7715	0.8552
<i>Barbara</i>	0.6177	0.8154	0.6978	0.7547	0.5470	0.8851
<i>Boat</i>	0.6518	0.7337	0.6670	0.7303	0.6032	0.7659
<i>Hill</i>	0.6566	0.7280	0.6579	0.7085	0.5313	0.7463
<i>Couple</i>	0.6711	0.7564	0.6989	0.7591	0.5639	0.7827
<i>Tiger</i>	0.6710	0.7360	0.6865	0.6974	0.5952	0.7473
<i>Zebra</i>	0.5938	0.6855	0.6174	0.6704	0.5575	0.7039
<i>Leopard</i>	0.6647	0.7265	0.6589	0.8333	0.7800	0.8534

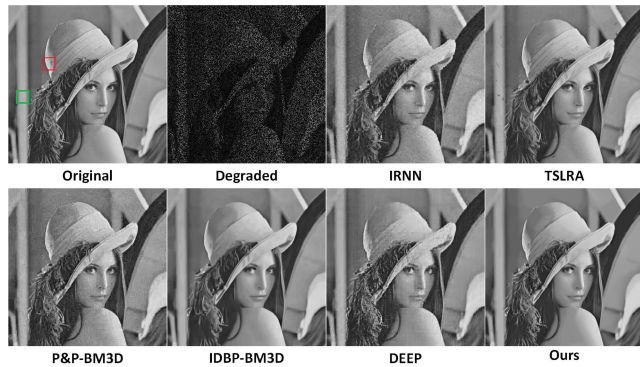
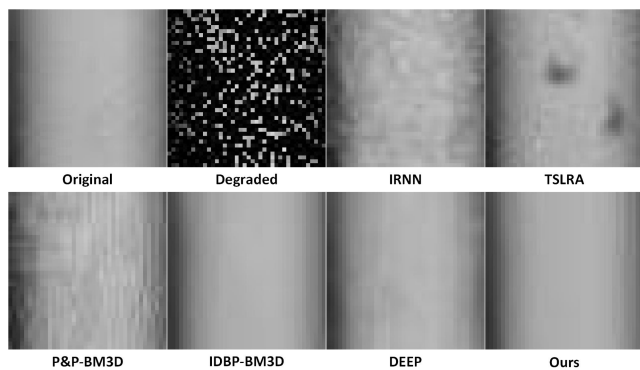
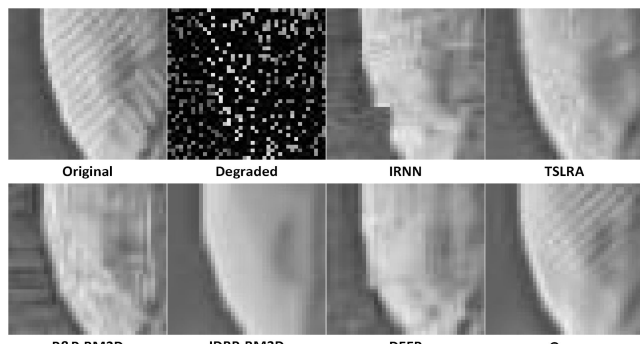
TABLE 3. PSNR results with 0.8 loss rate and noise level of 20.

	IRNN	TSLRA	P&P-BM3D	IDBP-BM3D	DEEP	Ours
<i>C.man</i>	20.63	23.67	21.15	24.01	17.23	24.23
<i>House</i>	23.56	27.01	23.30	29.18	18.69	30.11
<i>Peppers</i>	21.98	24.98	21.69	25.72	18.48	26.12
<i>Monarch</i>	20.46	24.03	20.84	24.07	17.50	24.76
<i>Lena</i>	23.63	27.04	23.13	28.29	19.09	28.82
<i>Barbara</i>	20.95	26.27	21.08	24.22	18.61	27.46
<i>Boat</i>	22.62	25.64	22.25	25.63	18.79	25.85
<i>Hill</i>	23.30	26.28	22.68	26.68	19.48	26.84
<i>Couple</i>	22.67	25.65	22.30	25.53	18.73	25.99
<i>Tiger</i>	21.38	24.05	21.26	23.61	19.70	23.86
<i>Zebra</i>	18.54	22.15	19.62	21.57	19.02	22.34
<i>Leopard</i>	22.03	24.07	21.59	24.28	22.61	24.52

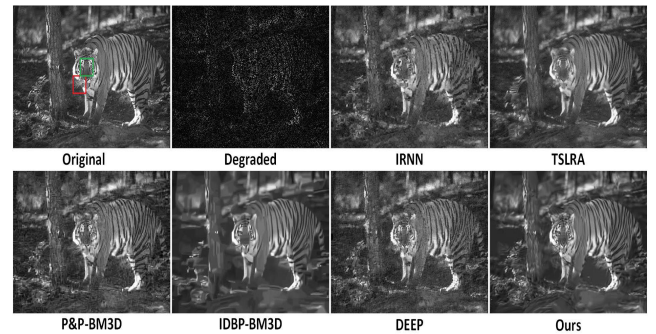
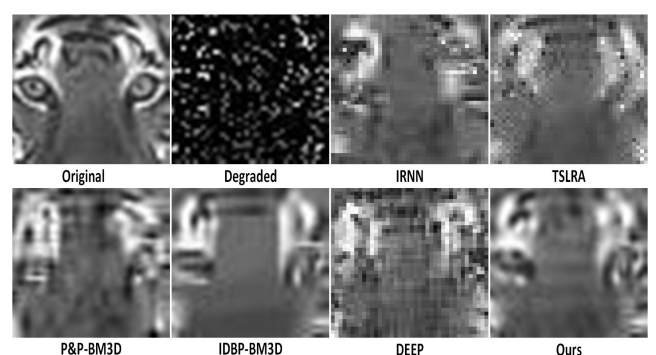
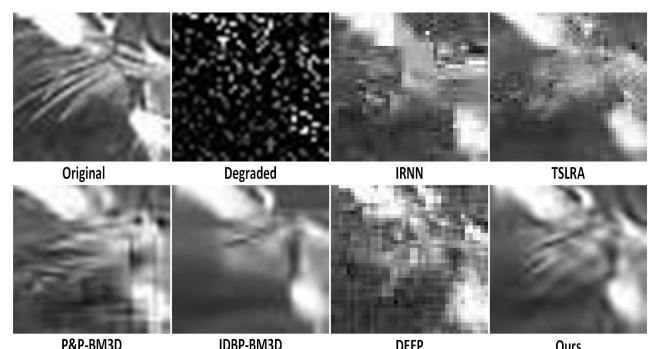
TABLE 4. SSIM results with 0.8 loss rate and noise level of 20.

	IRNN	TSLRA	P&P-BM3D	IDBP-BM3D	DEEP	Ours
<i>C.man</i>	0.4082	0.5432	0.4061	0.7488	0.2178	0.7504
<i>House</i>	0.4452	0.5827	0.4126	0.8178	0.2093	0.8318
<i>Peppers</i>	0.5037	0.6371	0.4679	0.7800	0.3027	0.7887
<i>Monarch</i>	0.5360	0.6810	0.5085	0.7953	0.3337	0.8199
<i>Lena</i>	0.4478	0.5874	0.4108	0.7909	0.2111	0.8123
<i>Barbara</i>	0.4341	0.6750	0.4318	0.6779	0.2858	0.8153
<i>Boat</i>	0.4590	0.5886	0.4295	0.6699	0.2532	0.6809
<i>Hill</i>	0.4535	0.5829	0.4209	0.6529	0.2488	0.6637
<i>Couple</i>	0.4736	0.6198	0.4639	0.6729	0.2758	0.7046
<i>Tiger</i>	0.4956	0.6181	0.4738	0.6328	0.3789	0.6513
<i>Zebra</i>	0.4396	0.5590	0.4181	0.6149	0.3533	0.6438
<i>Leopard</i>	0.4406	0.5461	0.4053	0.7772	0.7243	0.8130

To further compare these inpainting algorithms, we show the filling visual renderings of the Lena image and the Tiger image with a noise level of 10 and the Barbara image with

**FIGURE 4.** Inpainting results of different algorithms for Lena.**FIGURE 5.** Closeups of the green quadratate region in Fig.4.**FIGURE 6.** Closeups of the red quadratate region in Fig.4.

a noise level of 20, respectively. For the Lena image, Fig.4 shows the reference image and the degradation diagram with the noise level 10 and loss rate 0.8 of the Lena image. And shows the filled visual effect of these algorithms. To further compare these filling algorithms, we extracted the green and red areas similar to the original image(Fig.4) from the filling renderings of these comparison algorithms, and enlarge them for comparison. The enlarged green quadratate regions are shown in Fig.5, and the enlarged red quadratate regions are shown in Fig.6. For the Tiger image, Fig.7 shows the reference image and the degradation diagram with the noise level 10 and loss rate 0.8 of the Tiger image. And shows the

**FIGURE 7.** Inpainting results of different algorithms for Tiger.**FIGURE 8.** Closeups of the green quadratate region in Fig.7 .**FIGURE 9.** Closeups of the red quadratate region in Fig.7 .

filled visual effect of these algorithms. The enlarged green quadratate regions are shown in Fig.8, and the enlarged red quadratate regions are shown in Fig.9. For the Barbara image, Fig.10 shows the reference image and the degradation diagram with the noise level 20 and loss rate 0.8 of the Barbara image. And shows the filled visual effect of these algorithms. The enlarged green quadratate regions are shown in Fig.11, and the enlarged red quadratate regions are shown in Fig.12.

In terms of visual quality, the inpainting results on the structure or texture of IRNN, P&P-BM3D, and DEEP algorithms are inferior to those of the other three algorithms. Although IDBP-BM3D algorithm has an advantage over IRNN algorithm, P&P-BM3D and DEEP algorithm

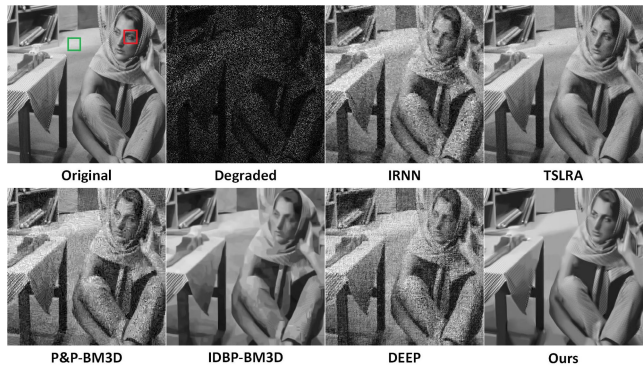


FIGURE 10. Inpainting results of different algorithms for Barbara.

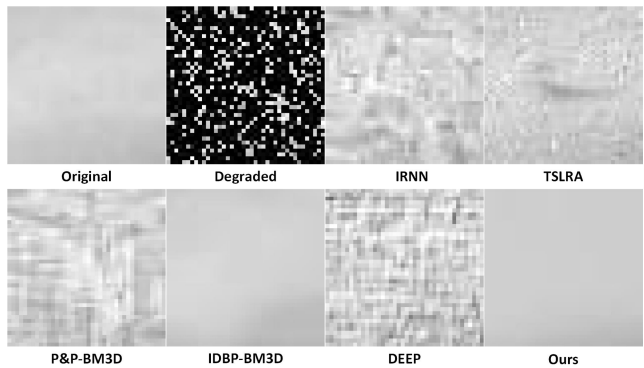


FIGURE 11. Closeups of the green quadratate region in Fig.10.

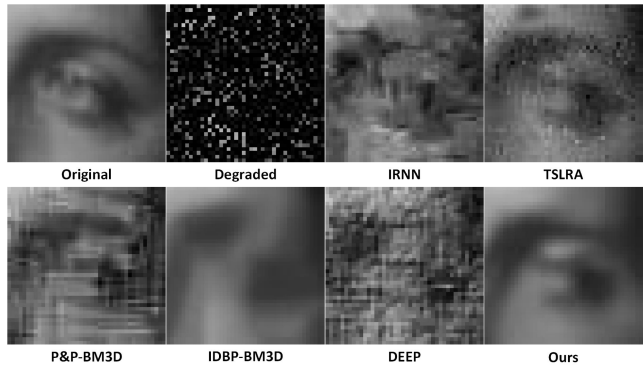


FIGURE 12. Closeups of the red quadratate region in Fig.10.

in structure, comparing to the other two algorithms, IDBP-BM3D algorithm fixes texture areas that are smoother. For example, Lena's hat in Fig.6, Tiger's beard in Fig.9 and Barbara's eyes in Fig.12. Through the above numerical analysis, we know that the PSNR value of the TSLRA algorithm is occasionally slightly higher than that of our method, especially for the images with rich texture, such as Tiger. However, by comparing the visual quality of the two methods, we find that not only in the flat areas (the Tiger's eyes in Fig.8), but also in the textured areas (the Tiger's beard in Fig.9), the filling effect through our method is more complete and clear. In the experimental results of these test images,

we find that the repair result of the flat area by the TSLRA algorithm is not complete, and there is a bump in the flat area of the repaired image, such as the floor next to the bookcase of image Barbara in Fig.10. In summary, both in terms of quantitative two index values and visual quality, the proposed algorithm shows strong inpainting capability, generating visually much more appropriate inpainting outputs.

V. CONCLUSION

In this paper, a new filling algorithm is proposed to complete the image inpainting task. This method approximates the image to a low-rank matrix by using the low-rank prior information of the image. By assigning different weights to the singular values of the matrix, the proposed algorithm improves the collaborative hard threshold of the BM3D algorithm, and combines with the advanced sparse coding reweighting mechanism. Finally, the degraded image is successfully constructed. The algorithm not only retains the structural information of the image but also fully repairs the detailed information of the image. And the proposed algorithm takes fewer iterations than the IDBP-BM3D algorithm. Besides, the proposed algorithm has higher index values than the IDBP-BM3D algorithm and generates much more pleasant visual quality over other related advanced algorithms.

REFERENCES

- [1] A. Evgeniou and M. Pontil, "Multi-task feature learning," in *Proc. Adv. Neural Inf. Process. Syst.*, Dec. 2007, pp. 41–48.
- [2] C. Tomasi and T. Kanade, "Shape and motion from image streams under orthography: A factorization method," *Int. J. Comput. Vis.*, vol. 9, no. 2, pp. 137–154, Nov. 1992.
- [3] M. Mesbahi and G. P. Papavassiliopoulos, "On the rank minimization problem over a positive semidefinite linear matrix inequality," *IEEE Trans. Autom. Control*, vol. 42, no. 2, pp. 239–243, Feb. 1997.
- [4] Y. S. Moon, P. Park, W. H. Kwon, and Y. S. Lee, "Delay-dependent robust stabilization of uncertain state-delayed systems," *Int. J. Control*, vol. 74, no. 14, pp. 1447–1455, Jan. 2001.
- [5] J. Abernethy, F. Bach, T. Evgeniou, and J.-P. Vert, "A new approach to collaborative filtering: Operator estimation with spectral regularization," *J. Mach. Learn. Res.*, vol. 10, pp. 803–826, Mar. 2009.
- [6] Y.-Q. Zhao and J. Yang, "Hyperspectral image denoising via sparse representation and low-rank constraint," *IEEE Trans. Geosci. Remote Sens.*, vol. 53, no. 1, pp. 296–308, Jan. 2015.
- [7] Y. Zhao and J. Yang, "Hyperspectral image denoising via sparsity and low rank," in *Proc. IEEE Int. Geosci. Remote Sens. Symp. (IGARSS)*, Jul. 2013, pp. 1091–1094.
- [8] W. Dong, G. Li, G. Shi, X. Li, and Y. Ma, "Low-rank tensor approximation with Laplacian scale mixture modeling for multiframe image denoising," in *Proc. IEEE Int. Conf. Comput. Vis. (ICCV)*, Dec. 2015, pp. 442–449.
- [9] W. He, H. Zhang, L. Zhang, and H. Shen, "Hyperspectral image denoising via noise-adjusted iterative low-rank matrix approximation," *IEEE J. Sel. Topics Appl. Earth Observ. Remote Sens.*, vol. 8, no. 6, pp. 3050–3061, Jun. 2015.
- [10] J. Xu, L. Zhang, D. Zhang, and X. Feng, "Multi-channel weighted nuclear norm minimization for real color image denoising," in *Proc. IEEE Int. Conf. Comput. Vis. (ICCV)*, Oct. 2017, pp. 1096–1104.
- [11] Y. Chang, L. Yan, and S. Zhong, "Hyper-laplacian regularized unidirectional low-rank tensor recovery for multispectral image denoising," in *Proc. IEEE Conf. Comput. Vis. Pattern Recognit. (CVPR)*, Jul. 2017, pp. 4260–4268.
- [12] N. Boumal and P. A. Absil, "RTRMC: A Riemannian trust-region method for low-rank matrix completion," in *Proc. Adv. Neural Inf. Process. Syst.*, 2011, pp. 406–414.
- [13] R. H. Keshavan, A. Montanari, and S. Oh, "Matrix completion from a few entries," *IEEE Trans. Inf. Theory*, vol. 56, no. 6, pp. 2980–2998, Jun. 2010.

- [14] K. Lee and Y. Bresler, "ADMiRA: Atomic decomposition for minimum rank approximation," *IEEE Trans. Inf. Theory*, vol. 56, no. 9, pp. 4402–4416, Sep. 2010.
- [15] C. Lu, J. Tang, S. Yan, and Z. Lin, "Generalized nonconvex nonsmooth low-rank minimization," in *Proc. IEEE Conf. Comput. Vis. Pattern Recognit.*, Jun. 2014, pp. 4130–4137.
- [16] E. J. Candès and B. Recht, "Exact matrix completion via convex optimization," *Found. Comput. Math.*, vol. 9, no. 6, pp. 717–772, Dec. 2009.
- [17] K.-C. Toh and S. Yun, "An accelerated proximal gradient algorithm for nuclear norm regularized linear least squares problems," *Pacific J. Optim.*, vol. 6, no. 3, pp. 615–640, Nov. 2010.
- [18] J.-F. Cai, E. J. Candès, and Z. Shen, "A singular value thresholding algorithm for matrix completion," *SIAM J. Optim.*, vol. 20, no. 4, pp. 1956–1982, Jan. 2010.
- [19] Z. Lin, M. Chen, and Y. Ma, "The augmented Lagrange multiplier method for exact recovery of corrupted low-rank matrices," Coordinated Sci. Lab., Urbana, IL, USA, Tech. Rep. UILU-ENG-09-2215, DC-247, 2009.
- [20] Z. Lin, A. Ganesh, J. Wright, and L. Wu, "Fast convex optimization algorithms for exact recovery of a corrupted low-rank matrix," Coordinated Sci. Lab., Urbana, IL, USA, Tech. Rep. UILU-ENG-09-2214, DC-246, Aug. 2009.
- [21] W. Dai and O. Milenkovic, "SET: An algorithm for consistent matrix completion," in *Proc. IEEE Int. Conf. Acoust., Speech Signal Process.*, Mar. 2010, pp. 3646–3649.
- [22] S. Ma, D. Goldfarb, and L. Chen, "Fixed point and Bregman iterative methods for matrix rank minimization," *Math. Program.*, vol. 128, nos. 1–2, pp. 321–353, Jun. 2011.
- [23] C. Chen, B. He, and X. Yuan, "Matrix completion via an alternating direction method," *IMA J. Numer. Anal.*, vol. 32, no. 1, pp. 227–245, Jan. 2012.
- [24] M. Yuan, V. R. Joseph, and H. Zou, "Structured variable selection and estimation," *Ann. Appl. Statist.*, vol. 3, no. 4, pp. 1738–1757, Dec. 2009.
- [25] Y. Ma and L. Zhi, "The minimum-rank gram matrix completion via modified fixed point continuation method," in *Proc. 36th Int. Symp. Symbolic Algebraic Comput. (ISSAC)*, 2011, pp. 241–248.
- [26] P. Jain, P. Netrapalli, and S. Sanghavi, "Low-rank matrix completion using alternating minimization," in *Proc. 45th Annu. ACM Symp. Theory Comput. (STOC)*, Jun. 2013, pp. 665–674.
- [27] Q. Guo, S. Gao, X. Zhang, Y. Yin, and C. Zhang, "Patch-based image inpainting via two-stage low rank approximation," *IEEE Trans. Vis. Comput. Graphics*, vol. 24, no. 6, pp. 2023–2036, Jun. 2018.
- [28] S. V. Venkatakrishnan, C. A. Bouman, and B. Wohlberg, "Plug-and-play priors for model based reconstruction," in *Proc. IEEE Global Conf. Signal Inf. Process.*, Dec. 2013, pp. 945–948.
- [29] T. Tirer and R. Giryes, "Image restoration by iterative denoising and backward projections," *IEEE Trans. Image Process.*, vol. 28, no. 3, pp. 1220–1234, Mar. 2019.
- [30] E. Candes, M. Wakin, and S. Boyd, "Enhancing sparsity by reweighted ℓ_1 minimization," *J. Fourier Anal. Appl.*, vol. 14, no. 5, pp. 877–905, 2008.
- [31] S. Boyd, "Distributed optimization and statistical learning via the alternating direction method of multipliers," *Found. Trends Mach. Learn.*, vol. 3, no. 1, pp. 1–122, 2010.
- [32] L. Mirsky, "A trace inequality of john von neumann," *Monatshefte für Math.*, vol. 79, no. 4, pp. 303–306, Dec. 1975.
- [33] S. Osher, M. Burger, D. Goldfarb, J. Xu, and W. Yin, "An iterative regularization method for total variation-based image restoration," *Multiscale Model. Simul.*, vol. 4, no. 2, pp. 460–489, Jan. 2005.
- [34] V. Lempitsky, A. Vedaldi, and D. Ulyanov, "Deep image prior," in *Proc. IEEE/CVF Conf. Comput. Vis. Pattern Recognit.*, Jun. 2018, pp. 9446–9454.



SHUMEI WANG received the B.S. degree from the School of Nursing, Weifang Medical University. She is currently the Deputy Head Nurse with the Department of General Surgery, Yidu Central Hospital of Weifang. Her research interest is nursing methods for breast cancer.



SHUJUN FU received the B.S. degree in power engineering and the M.S. degree in computational mathematics from Shandong University, in 1990 and 1999, respectively, and the Ph.D. degree in signal and information processing from Beijing Jiaotong University, in 2009. He is currently a Professor with the Department of Mathematics, Shandong University. He has authored about 60 papers in important journals and conferences. His research interests include image processing, partial differential equations, numerical computing, medical imaging, image measurement, and target detection and recognition. He is also a Peer Reviewer on some important journals.



YULIANG LI graduated from Shandong Medical University, in 1993, and received the M.D. degree from the Huazhong University of Science and Technology, in 2001. He is currently the Director of the Interventional Medicine Department, Second Hospital of Shandong University, and also the Professor and Doctoral Supervisor of Shandong University. He has authored about 30 articles in important journals and conferences. His research interests include various hemorrhagic diseases, ischemic diseases, neoplastic diseases, and medical image processing. He is also a Peer Reviewer on some important journals.



SHOUIYI LIU is currently pursuing the bachelor's degree with the Department of Electrical and Electronic Engineering, Xi'an Jiaotong-Liverpool University. His research interests include image processing, unmanned aerial vehicles, and remote communication.



WEIFENG ZHOU is currently an Associate Professor with the Department of Mathematics and Physics, Qingdao University of Science and Technology. She has authored about 20 papers in important journals and conferences. Her research interests include image processing and medical reconstruction.



RUYI HAN received the B.S. degree from the Department of Mathematics, Taiyuan Teachers College, Taiyuan, China, in 2014, and the M.S. degree from the School of Mathematics, Taiyuan University of Technology, Taiyuan, in 2018. She is currently pursuing the Ph.D. degree with the School of Mathematics, Shandong University, Jinan, China. Her research interests include medical image processing and pattern recognition, especially image inpainting.